1. Norsaidah MUHAMAD NADZIR[1], 2. Mohamad Kamal A. RAHIM[1], 3. Mohamed HIMDI[2], 4. Noor Asniza MURAD[1], 5. Osman AYOP[1]

Faculty of Electrical Engineering, Universiti Teknologi Malaysia, Johor Bahru, Malaysia (1), Institute of Electronics and Telecommunications of Rennes IETR, University of Rennes 1, Rennes, France (2)
ORCID: 1. 0000-0003-4117-9433; 2. 0000-0002-5488-9277; 3. 0000-0002-0529-4656; 4. 0000-0002-5685-3040; 5. 0000-0001-8162-7398

doi:10.15199/48.2024.03.38

Effect of CSRR Rotation on Size and Polarization of Antenna

Abstract. *This paper describes the design and development of microstrip patch antenna with circular metamaterial structure at the ground plane that will be rotated multiple times at an incremental angle of 22.5°. There are several benefits that result from the introduction of the metamaterial structure rotated to various angles to the patch antenna such as increased number of frequencies, increased efficiency and gain at lower frequencies, reduced size antenna, and changed polarization. The antenna is also horizontally polarized at lower frequencies with high gain and efficiency when the metamaterial structure is rotated to 22.5° and 45° while operational at only one lower frequency for 67.5°. These responses are confirmed through the standard antenna measurement process.*

Streszczenie. *Tento článek popisuje návrh a vývoj mikropáskové flíčkové antény s kruhovou metamateriálovou strukturou na zemní ploše, která bude několikrát natočena pod úhlem 22,5°. Existuje několik výhod, které vyplývají ze zavedení struktury metamateriálu natočené do různých úhlů k flíčkové anténě, jako je zvýšený počet frekvencí, zvýšená účinnost a zisk na nižších frekvencích, zmenšená velikost antény a změněná polarizace. Anténa je také horizontálně polarizována na nižších frekvencích s vysokým ziskem a účinností, když je metamateriálová struktura otočena o 22,5° a 45° při provozu pouze na jedné nižší frekvenci pro 67,5°. Tyto odezvy jsou potvrzeny standardním procesem měření antény. (**Wpływ rotacji CSRR na rozmiar i polaryzację anteny**)*

Keywords: Microstrip patch antenna, metamaterial, split ring resonator, rotation.
Słowa kluczowe: Mikropásková anténa, metamateriál, dělený prstencový rezonátor, rotace.

Introduction

Microstrip patch antenna is widely used and popular in communication systems due to its benefits such as design simplicity, ease of integration and low cost. Microwave frequency patch antennas often have miniature characteristics and are usually small enough to be integrated with current systems. However, with recent technology and system advancement, it is imperative for the antenna to be able to radiate at multiple frequencies to cater to different applications and retain its compact size. There are numerous techniques to enhance the performance of a patch antenna, either by modifying the size or shape of the radiating element or both. For example, it is widely recognized that incorporating a split ring resonator (SRR) or other metamaterial structure into a patch antenna is an effective approach to raise the number of radiating frequencies and minimizing the antenna's physical size [1–4]. Additionally, research has demonstrated that the implementation of complementary split ring resonator (CSRR) structures can effectively mitigate mutual coupling in a linear array antenna [5-7] and in MIMO antennas [8,9]. The CSRR structure in antennas could also introduce wideband characteristics based on [10] and [11]. To further acknowledge the benefit of SRR structures in communication system, the effect of integrating CSRR structure with simple patch antenna is presented.

To increase the number of resonant frequencies and achieve compact size antenna, a slotted single element microstrip patch antenna (MPA) designed to operate at 26 GHz is modified by adding a circular electrically small metamaterial structure, such as a CSRR, to its ground plane. This modification enables the antenna to achieve dual frequency operation, covering both the 26 GHz and 28 GHz frequency bands. Then, the circular CSRR is rotated to an increment angle of 22.5° to achieve further size reduction and distinct polarization. The first part describes the development of a slotted MPA at 26 GHz. Then, the development and study of the interaction between the MPA with circular CSRR is discussed and finally, the comparison of the developed antennas simulated and measured results is shown, followed by conclusions.

Microstrip Patch Antenna at 26 GHz

This section outlines the construction of a 26 GHz MPA and the incorporation of a CSRR structure into the antenna. The entire simulation process is conducted using the Computer Simulation Technology (CST) software. Fig. 1 illustrates the simulation model of the slotted MPA. The substrate measures 20 mm × 20 mm, while the patch measures 3.7 mm × 3.7 mm. The direct feeding method using an inset feed technique is applied to obtain maximum input impedance matching [12]. The antenna is designed on an RT/Duroid 5880 substrate, characterized by a relative permittivity (εr) of 2.2 and a dissipation factor (tan δ) of 0.0009. Table 1 summarizes the parameter list of the MPA at 26 GHz.

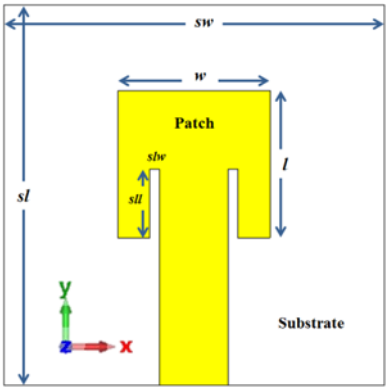

Fig.1. Simulation model of the slotted MPA at 26 GHz.

Table 1. Parameter of the slotted MPA at 26 GHz.

Parameter	Value [mm]
Width of substrate, *sw*	20
Length of substrate, *sl*	20
Thickness of substrate, *h*	0.508
Width of patch, *w*	3.7
Length of patch, *l*	3.7
Width of slot, *slw*	0.2
Length of slot, *sll*	1.45
Thickness of copper, *t*	0.035

Microstrip Patch Antenna with Circular Complementary Split Ring Resonator

A simple microstrip patch antenna generally produces a single resonating frequency based on the parameter of the antenna. The number of resonant frequencies for patch antennas can be increased using a variety of methods. The integration of a split ring resonator (SRR) into the antenna design is one of them. The splits at the end of the ring and the space between the rings in the SRR structure cause magnetic resonance. Then, the charges preventing the currents from circling the ring would prevent the induced resonant currents from flowing along the rings [13–16]. Finally, the circuit is completed across the small capacitive gap between the rings [17–22]. The simulation model and their equivalent circuits of SRR and CSRR are displayed in Fig. 2 and Fig. 3.

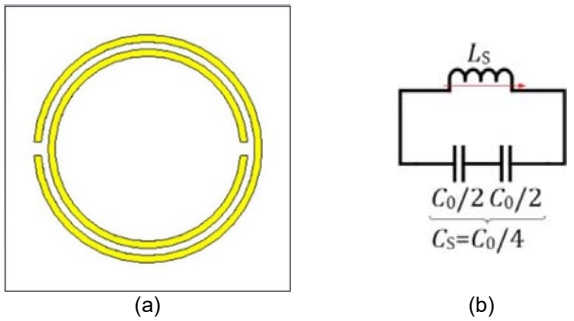

(a) (b)

Fig.2. Simulation model of (**a**) SRR structure and its (**b**) equivalent circuit [3].

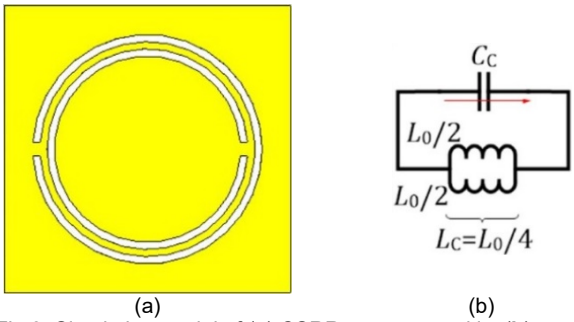

(a) (b)

Fig.3. Simulation model of (**a**) CSRR structure and its (**b**) equivalent circuit [3].

To create oscillating currents between the two rings of the SRR, an axial magnetic field is used, which then excites the component. The resonance produced by these currents prevents signal propagation at that frequency. Axial electric field is used to excite its complementary structure, CSRR, and produce stop band [13, 14]. Referring to Figure 4, the resonant frequency of the electrically small metamaterial, SRR as described by Marqués, Martin, and Sorolla are shown in Equation (1–5) below:

(1) $$f_{srr} = \frac{1}{2\pi\sqrt{L_s C_s}}$$

(2) $$L_s = 0.0002l\left(2.303log_{10}\left[\frac{4l}{c}\right] - 2.45l\right)\mu H$$

(3) $$C_s = \left[\frac{\pi r_{avg} C_{pul}}{2} + \frac{\epsilon_0 ch}{2g}\right]$$

where L_s is the effective inductance, C_s is the effective capacitance, l is the length of outer ring, c is the length of inner ring, C_{pul} is the capacitance between the inner and outer split rings of the resonator per unit length, r_{avg} is the average radius of the split ring, g is the gap between the split ring, and h is the thickness of the substrate. Next, referring to Figure 3:

(4) $$C_c = 4\left(\frac{\epsilon_0}{\mu_0}\right)L_s$$

(5) $$C_0 = 4\left(\frac{\epsilon_0}{\mu_0}\right)L_0$$

The values of effective capacitance and inductance for CSRR structure, L_c and C_c can be calculated by modifying the equation above. Finally, the resonant frequency of CSRR (f_{csrr}) can be calculated using equation (6).

(6) $$f_{csrr} - \frac{1}{2\pi\sqrt{L_c C_c}}$$

Figure 4 depicts the position and parameters of the CSRR structure on the ground plane of the outlined patch antenna, and Table 2 lists the values of the parameter following performance optimization of the antenna.

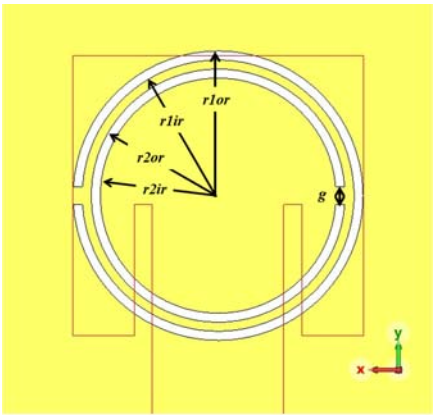

Fig.4. Parameters of the CSRR.

Table 2. Parameter of the slotted MPA at 26 GHz.

Parameter	Value [mm]
Ring 1 outer radius, *r1or*	1.6
Ring 1 inner radius, *r1ir*	1.5
Ring 2 outer radius, *r2or*	1.4
Ring 2 inner radius, *r2ir*	1.3
Ring split gap, *g*	0.2

Next, the CSRR structure is rotated to 22.5°, 45°, and 67.5° for various operating frequency with distinct polarization at each frequency.

Results and Discussion

This section is divided into two parts. The first part discusses the performance of the MPA after integrating the CSRR structure. This result is to set a benchmark for the subsequent result of the rotation of the CSRR. The next part discusses the performance of the antenna when the CSRR structure is rotated at various angles.

Microstrip Patch Antenna with Circular Complementary Split Ring Resonator

The introduction of an electrically small metamaterial structure to the antenna's ground plane reduces the patch size by 27.53%, from 3.7 mm × 3.7 mm to 3.2 mm × 3.1 mm to maintain operational frequency at 26 GHz. Fig. 8 depicts the ground plane of the fabricated antenna, with CSRR structure at 0° etched out of the ground plane. On the other hand, Fig. 9 shows the comparison between the simulated and measured reflection coefficient, S11, of the MPA integrated with the circular CSRR. From the graph, the measured result is in good agreement with the simulated result, with a slight shift to the right. This shift is due to the nature of millimetre wave antennas that are highly sensitive to its dimension which means small deviation on the fabricated dimension from the simulated dimension could result in significant difference on the measured performance of the antenna.

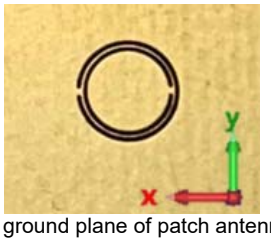

Fig.8. CSRR on the ground plane of patch antenna.

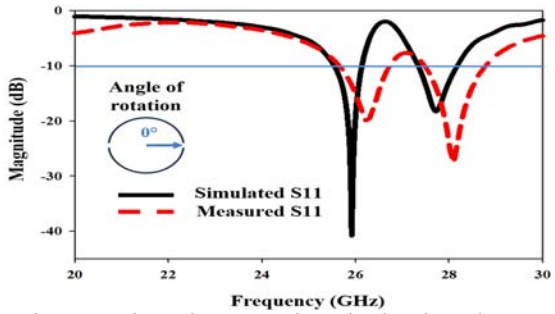

Fig.9. A comparison between the simulated and measured reflection coefficient, S11, of the MPA with CSRR.

The comparison of simulation results presented in Fig. 10 and Fig. 11 reveals that the inclusion of the CSRR structure on the antenna's ground plane (indicated as 0°) leads to a noteworthy improvement in antenna efficiency. Specifically, at 28 GHz frequency, the antenna demonstrates a substantial gain increase of 3.33 dB. On the other hand, there is 3.35 dB gain loss and a slight drop in antenna efficiency at 26 GHz which is due to patch size reduction and the defected ground plane.

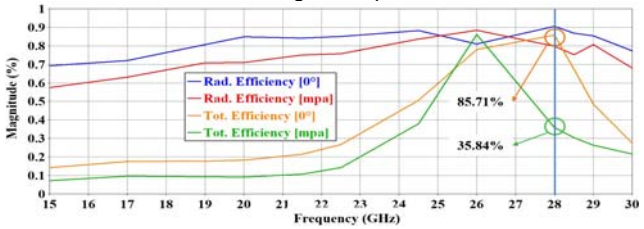

Fig.10. Comparison of simulated efficiency of the MPA and MPA with circular CSRR.

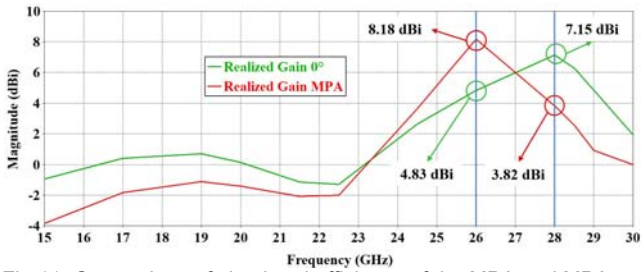

Fig.11. Comparison of simulated efficiency of the MPA and MPA with circular CSRR.

Next, Fig. 12(a) shows the co-polarization plot (Eφ) and cross-polarization plot (Eθ) of the antenna at H-plane (φ = 0°) for both matched frequencies. Fig. 12(b) shows the co-polarization plot (Eθ) and cross-polarization plot (Eφ) of the antenna at E-plane (φ = 90°). Since the value of the radiation at co-polarization plot is higher than the value at cross-polarization plot, the antenna is vertically polarized at both matched frequencies.

Fig. 13(a) and Fig. 13(b) shows the comparison between the simulated and measured radiation patterns of the antenna at 28 GHz in the H-plane and E-plane, respectively. The measured results align well with the simulated results, validating the accuracy of the simulation and indicating a successful proof of concept for the antenna design.

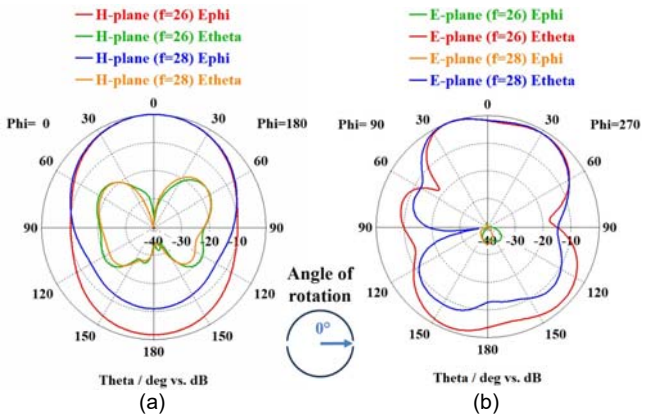

(a) (b)

Fig.12. Comparison between simulated and measured radiation pattern of MPA at 26 GHz at (**a**) H-plane (φ=0°, Eφ) and (**b**) E-plane (φ=90°, Eθ).

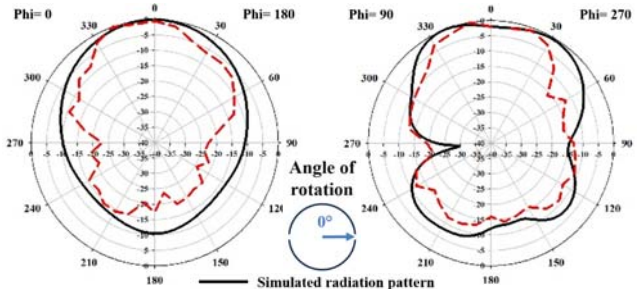

(a) (b)

Fig.13. Comparison between simulated and measured radiation pattern of MPA at 26 GHz at (**a**) H-plane (φ=0°, Eφ) and (**b**) E-plane (φ=90°, Eθ).

Effect of Rotation of the CSRR Structure

In this part, the circular CSRR structure, which is positioned on the ground plane will be rotated several times and the performance of the antenna is discussed. First, the structure is rotated at 22.5° on the z-axis as shown in the ground plane of the fabricated antenna in Fig. 14. As a result, the number of resonating frequencies increased to three at 22.5 GHz, 26 GHz, and 28 GHz. The comparison between the simulated S11 and the measured result is as shown in Fig. 15. From the graph, the measured result shows a slight shift to the right. The frequency shift might be due to the slight change in the antenna parameter during fabrication since the dimension is quite small (0.1 mm difference between outer and inner radius of CSRR).

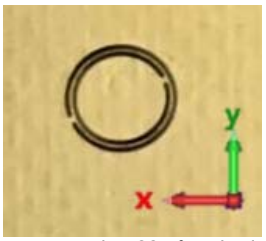

Fig.14. CSRR structure rotated at 22.5° etched on the ground plane of the fabricated patch antenna.

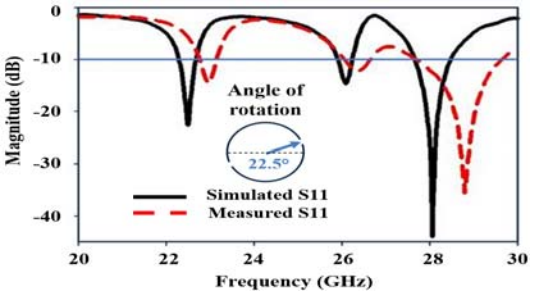

Fig.15. Comparison of the simulated and measured S11 reflection coefficients of the MPA with the CSRR rotated to 22.5°.

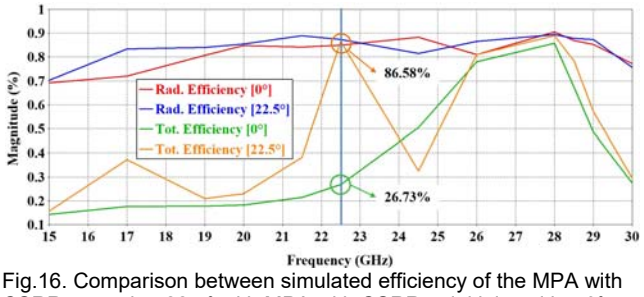

Fig.16. Comparison between simulated efficiency of the MPA with CSRR rotated to 22.5° with MPA with CSRR at initial position 0°.

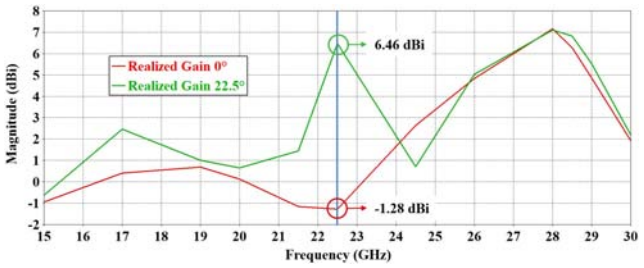

Fig.17. Comparison between simulated gain of the MPA with CSRR rotated to 22.5° with MPA with CSRR at initial position 0°.

Next, Fig. 16 shows the comparison between the simulated efficiency of the antenna at 0° and 22.5°. The graph shows that the 22.5° rotation of the CSRR on the antenna lead to an increase of efficiency at 22.5 GHz from 27% before rotation to 87% after the 22.5° rotation. This is supported by the significant increase in gain from -1.28 dB to 6.46 dB shown in Fig. 17. At frequencies of 26 GHz and 28 GHz, the antenna exhibited a gain of 5.02 dB and 7.09 dB, respectively. Furthermore, the antenna achieved an efficiency of 81% at 26 GHz and 89% at 28 GHz.

From the simulation result, the radiation pattern of the antenna shows an interesting behavior. Fig. 18(a) illustrates the radiation pattern of the antenna in the H-plane (φ=0°) for each matched frequency. The solid line represents the co-polarization plot (Eφ), while the dashed line represents the cross-polarization plot (Eθ) at each matched frequency. On the other hand, Fig. 18(b) displays the radiation pattern of the antenna in the E-plane (φ=90°) with the co-polarization plot (Eθ) depicted by a solid line and the cross-polarization plot (Eφ) represented by a dashed line for each matched frequency. The graphs show that at 22.5 GHz, the value of cross-polarization is higher than the value of co-polarization. At frequencies 26 GHz and 28 GHz, the radiation pattern of the antenna exhibits normal behaviour, with the co-polarization having higher values compared to the cross-polarization.

This means that when the CSRR structure is rotated to 22.5°, it not only maintains its functionality at 26 GHz and 28 GHz but also enables the antenna to achieve high efficiency and gain with horizontal polarization at 22.5 GHz. To measure the radiation pattern of the antenna at 22.5 GHz, the antenna is physically tilted 90° on the z-axis. Fig. 19(a) and Fig. 19(b) depict the comparison between the simulated and measured radiation patterns at 22.5 GHz in the H-plane and E-plane, respectively. The graph demonstrates that the measured results align well with the simulated results, indicating that the antenna is fully operational at this frequency.

Next, the metamaterial structure is rotated to 45° as shown in the ground plane of the fabricated antenna in Fig. 20. In Fig. 21, the comparison between the simulated and measured S11 is depicted. The antenna exhibits three resonating frequencies at 17 GHz, 21.5 GHz, and 28.5 GHz. From the graph, the measured result shows a slight shift to the right compared to the simulated result. It is important to note that millimetre wave antennas are highly sensitive to their dimensions, and even slight variations in fabrication parameters can lead to differences in performance, such as frequency shifts or reduced efficiency.

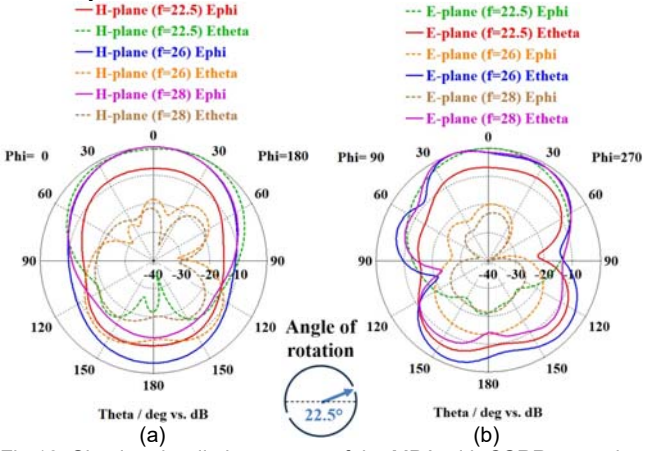

Fig.18. Simulated radiation pattern of the MPA with CSRR rotated at 22.5° at (**a**) H-plane (φ=0°) and at (**b**) E-plane (φ=90°).

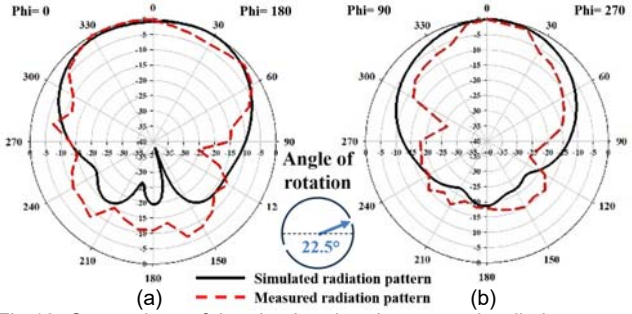

Fig.19. Comparison of the simulated and measured radiation patterns of the MPA with the CSRR rotated at 22.5° at 22.5 GHz at (**a**) H-plane (φ=0°, Eθ) and at (**b**) E-plane (φ=90°, Eφ).

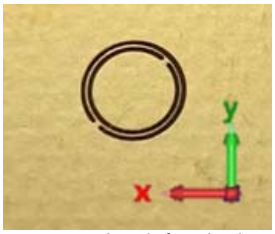

Fig.20. CSRR structure rotated at 45° etched on the ground plane of patch antenna.

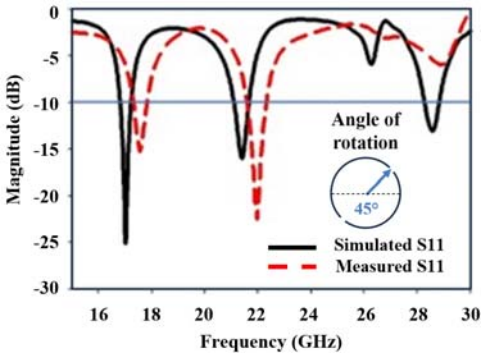

Fig.21. Comparison of the simulated and measured reflection coefficient, S11, of the MPA with a circular CSRR rotated to 45°.

Next, Fig. 22 shows the comparison of simulated efficiency between antenna with CSRR at 0° and the antenna with CSRR rotated at 45°. From the graph, the efficiency of the antenna at two lower frequencies increased

dramatically when the CSRR structure is rotated to 45°. The antenna attained 87.52% efficiency at 17 GHz and 87.54% efficiency at 21.5 GHz. This high efficiency led to an increase in gain as shown in Fig. 23 where the antenna obtained 5.28 dB and 6.14 dB gain for frequencies 17 GHz and 21.5 GHz respectively. At frequency 28.5 GHz, the antenna attains 7 dB gain with 87.64% efficiency.

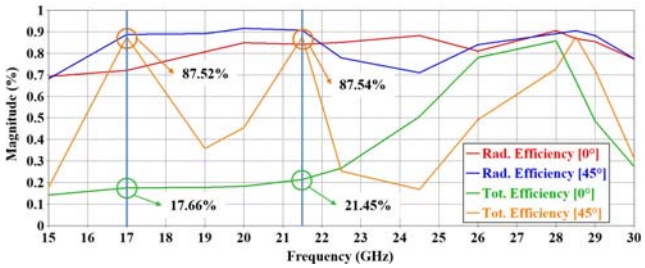

Fig.22. Comparison between simulated efficiency of MPA with CSRR rotated to 45° with 0°.

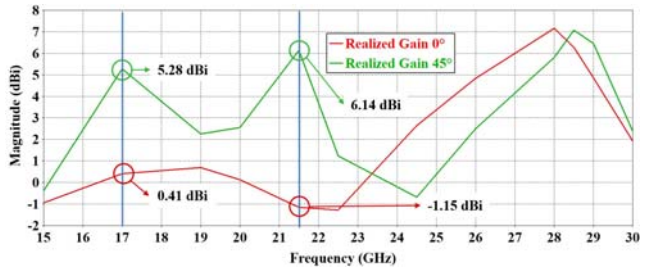

Fig.23. Comparison between simulated gain of the MPA with CSRR rotated to 45° with 0°.

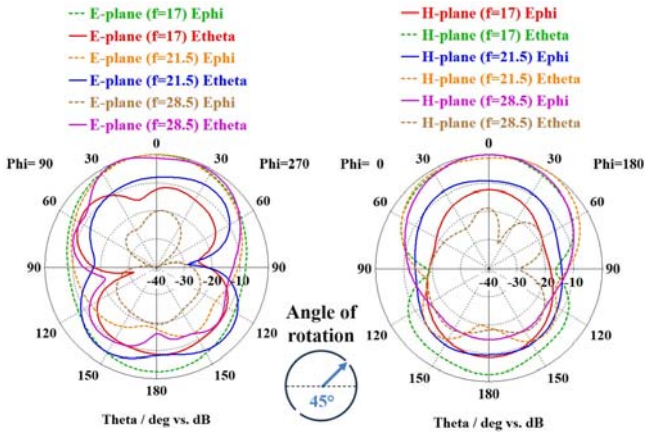

Fig.24. Simulated radiation pattern of the MPA with CSRR rotated at 45° at (**a**) H-plane (φ=0°) and at (**b**) E-plane (φ=90°).

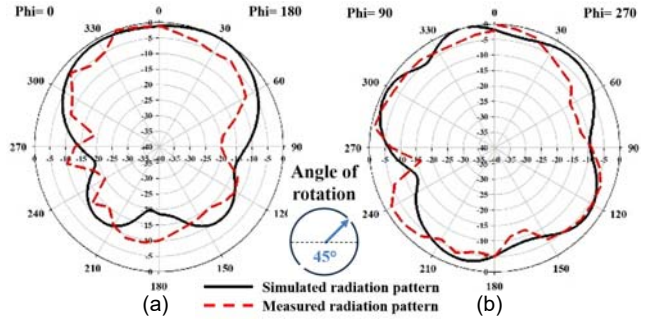

Fig.25. Comparison of the simulated and measured radiation patterns of the MPA with the 45°-rotated CSRR at 21.5 GHz at (**a**) H-plane (φ=0°, Eθ) and at (**b**) E-plane (φ=90°, Eφ).

Fig. 24 illustrates the radiation pattern of the antenna in the H-plane (φ = 0°) and E-plane (φ = 90°). In the H-plane, the solid line represents the co-polarization plot (Eφ), while the dashed lines represent the cross-polarization plot (Eθ). Referring to Figure 18(a), radiation pattern at H-plane for frequencies 17 GHz and 21.5 GHz indicates the value of Eφ is lower than the value of Eθ and at frequency 28.5 GHz, the value of Eθ is higher than the value of Eφ. Figure 18(b) shows the radiation pattern of the antenna at E-plane (φ = 90°) which also depicts the same information where the cross-polarization (Eφ) plot has higher value compared to the value of the co-polarization (Eθ) plot.

This result mainly indicates that at 17 GHz, a horizontally polarized, compact sized antenna with high gain is achievable just by rotating the CSRR structure on the ground plane of an MPA to 45°. Comparing the size of the patch antenna with CSRR rotated to 45° with a standard 17 GHz patch antenna, more than 70% size reduction can be attained. Plus, the antenna is also operational at 21.5 GHz frequency horizontally polarized, with high gain and efficiency even though the size reduction is not as significant. Fig. 25 displays a comparison of the simulated and measured radiation patterns at 21.5 GHz as proof of concept.

Finally, the CSRR structure is rotated to 67.5° as shown on the ground plane of the fabricated antenna in Fig. 26. This antenna also shows an interesting behavior because from the S11 plot in Fig. 27, the antenna shows only one radiating frequency at 20 GHz. Although the number of radiating frequencies of the antenna was reduced, the efficiency at frequency 20 GHz increased from 17.78% to 92.16% as shown in Fig. 28. Fig. 29 shows the antenna achieved a 6.12 dB gain increase at the same frequency compared to the antenna with CSRR at 0°.

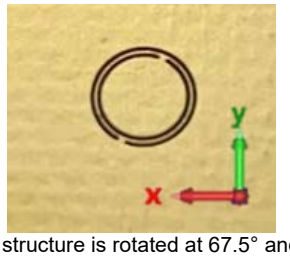

Fig.26. The CSRR structure is rotated at 67.5° and etched on the ground plane of the antenna.

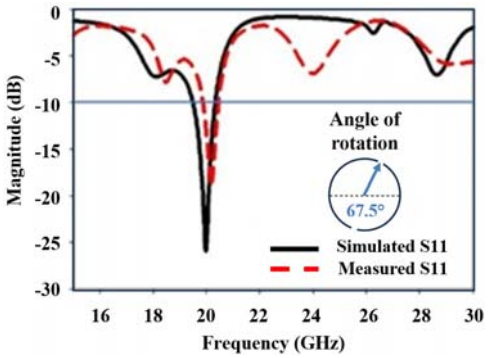

Fig.27. Comparison of simulated and measured reflection coefficient, S11, of the MPA with CSRR rotated to 67.5°.

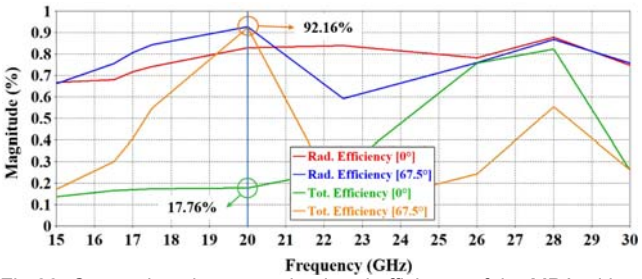

Fig.28. Comparison between simulated efficiency of the MPA with CSRR rotated to 67.5° with 0°.

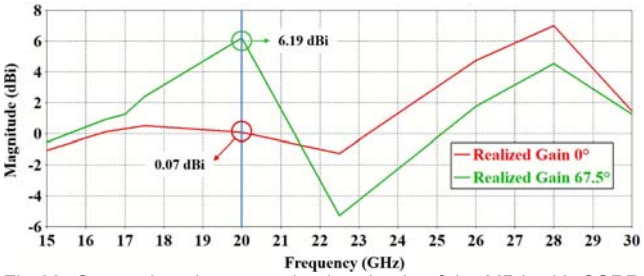

Fig.29. Comparison between simulated gain of the MPA with CSRR rotated to 67.5° with 0°.

In Fig. 30, the simulated radiation pattern at the H-plane (φ = 0°) and E-plane (φ = 90°) is presented. The graphs indicate that the value of the cross-polarization (Eθ in the H-plane and Eφ in the E-plane) is higher compared to the co-polarization (Eφ in the H-plane and Eθ in the E-plane) plot. This signifies that it is possible to achieve horizontally polarized, high efficiency antenna at 20 GHz with high gain, by rotating the CSRR structure on the ground plane of the antenna at 67.5°.

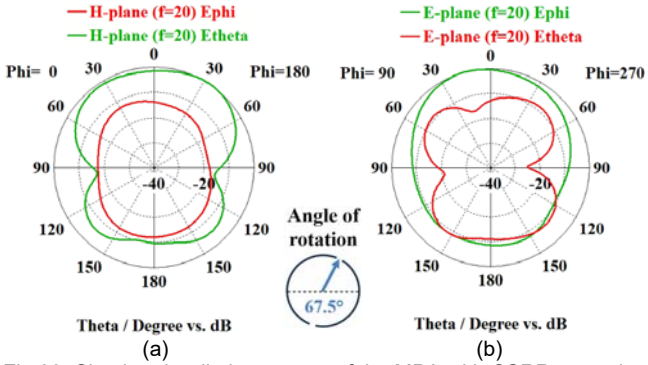

Fig.30. Simulated radiation pattern of the MPA with CSRR rotated at 67.5° at (**a**) H-plane (φ=0°) and at (**b**) E-plane (φ=90°).

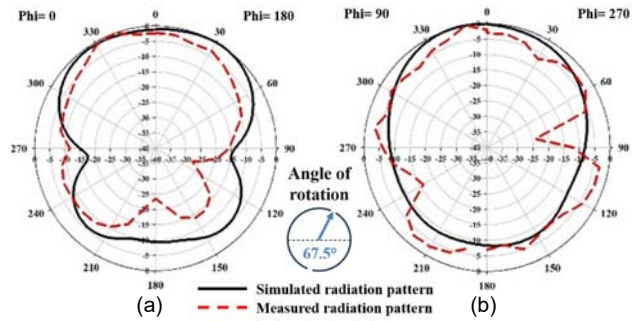

Fig.31. Comparison of the MPA's simulated and measured radiation patterns at 20 GHz with a 67.5°-rotated CSRR at (a) H-plane (φ=0°, Eθ) and at (**b**) E-plane (φ=90°, Eφ).

Table 3. Summary of the performance measurement of the MPA and MPA with CSRR rotated to multiple angles.

MPA with CSRR rotated at angle (°)	Polarization	Gain (dB)
MPA (without CSRR)	Vertical at 26 GHz	8.18
0°	Vertical at 26 GHz and 28 GHz	4.84, 7.15
22.5°	Horizontal at 22.5 GHz, Vertical at 26 GHz and 28 GHz	6.46, 5, 7
45°	Horizontal at 17 GHz and 21.5 GHz Vertical at 28.5 GHz	5.28, 6.13, 7

To evaluate the antenna's performance, the radiation pattern is measured by tilting the antenna to 90° on the z-axis. Fig. 31 displays the comparison between the simulated and measured radiation patterns at 20 GHz frequency. The graph demonstrates that the measured and simulated results exhibit good agreement. Finally, the summary of all the results achieved from the developed antennas are tabulated in Table 3.

Conclusion

This paper presents a miniaturized microstrip patch antenna with an electrically small metamaterial or a complementary split ring resonator and the effect of the rotation of the metamaterial structure to the performance of the antenna. The initial design involved creating a square microstrip patch antenna with a targeted radiation frequency of 26 GHz. Subsequently, the circular CSRR structure was integrated into the antenna's ground plane to achieve dual-band performance. As a result, the addition of the CSRR structure not only reduced the size of the patch antenna from 3.7 mm × 3.7 mm to 3.2 mm × 3.1 mm but also enabled the antenna to resonate at two frequencies, effectively increasing the number of resonating frequencies. When the metamaterial structure is rotated to 45°, the antenna managed to radiate at 17 GHz horizontally polarized with high efficiency and gain. Compared to a general 17 GHz patch antenna, a significant 70% size reduction is attained by rotating the metamaterial structure at the ground plane of a millimetre wave patch antenna to 45°. Plus, the antenna also managed to resonate at 21.5 GHz and 28.5 GHz frequency. Other than that, the antenna also successfully radiates at three different frequencies when the metamaterial structure is rotated to 22.5°. At 22.5 GHz, the antenna is horizontally polarized with high efficiency and gain and vertically polarized at 26 GHz and 28 GHz frequencies. Furthermore, when the metamaterial structure is rotated to 67.5°, the antenna is operational at only 20 GHz horizontally polarized with high efficiency and gain.

This work was supported in part by the Malaysian Ministry of Higher Education, Universiti Teknologi Malaysia, Research Management Centre, and Faculty of Electrical Engineering for the support of the research under Grant No. 09G19 and FRGS/1/2021/TKO/UTM/01/7.

***Authors**: Norsaidah Muhamad Nadzir, Mohamad Kamal A. Rahim, Noor Asniza Murad, Osman Ayop, Faculty of Electrical Engineering, Universiti Teknologi Malaysia, Johor Bahru, Malaysia E-mail: saidahnadzir@gmail.com, mdkamal@utm.my, asniza@fke.utm.my, and osman@fke.utm.my; Mohamed Himdi, Institute of Electronics and Telecommunications of Rennes IETR, University of Rennes 1, Rennes, France, E-mail: Mohamed.Himdi@univ-rennes.fr.*

REFERENCES

[1] El Yousfi, A., Lamkaddem, A., Abdalmalak, K.A., et al. A miniaturized triple-band and dual-polarized monopole antenna based on a CSRR perturbed ground plane. *IEEE Access*, (**2021**), 9, pp.164292-164299.

[2] Aminu-Baba, M., Rahim, M.K.A., Zubir, F., et al. Microstrip antenna with CSRR ground structure. *International Symposium on Antennas and Propagation (ISAP)*, **2017**, (pp. 1-2).

[3] Reddy, G.B. And Kumar, D.S. Miniaturization of microstrip slot antenna using SRR and CSRR loading. *3rd International Conference on Microwave and Photonics (ICMAP)*, **2018**, (pp. 1-2).

[4] Nadzir NM, Rahim MK, Himdi M, et al. Millimeter Wave Linear Array Microstrip Antenna with Circular CSRR. *International Symposium on Antennas and Propagation (ISAP)*, **2021** Oct 19 (pp. 1-2).

[5] Selvaraju, R., Jamaluddin, M.H., Kamarudin, M.R., et al. Mutual coupling reduction and pattern error correction in a 5G beamforming linear array using CSRR. *IEEE Access*, **2018**, 6, pp.65922-65934.

[6] Ni, C., Jiang, J., Wu, W.J., et al. Decoupling method based on complementary split ring resonator (CSRR) for two cone shipborne antennas. *IEEE Access*, **2021**, 9, pp.167845-167854.

[7] Chen L, Ma Q, Luo SS, et al. Touch-Programmable Metasurface for Various Electromagnetic Manipulations and Encryptions. *Small*, **2022**, 18(45):2203871.
[8] Nadeem, I., and Choi, D.Y. Study on mutual coupling reduction technique for MIMO antennas. *IEEE Access*, **2018**, 7, pp.563-586.
[9] Wang, Z., Li, C. and Yin, Y. A meta-surface antenna array decoupling (MAAD) design to improve the isolation performance in a MIMO system. *IEEE Access*, **2020**, 8, pp.61797-61805.
[10] Feng, S., Zhang, L., Yu, H.W., et al. A single-layer wideband differential-fed microstrip patch antenna with complementary split-ring resonators loaded. *IEEE Access*, **2019**, 7, pp.132041-132048.
[11] Bilal, R.M.H., Baqir, M.A., Choudhury, P.K., et al. Wideband microwave absorber comprising metallic split-ring resonators surrounded with E-shaped fractal metamaterial. *IEEE Access*, **2021**, 9, pp.5670-5677.
[12] M. S. Islam, M. I. Ibrahimy, S. M. A. Motakabber, et al. A Rectangular Inset-Fed Patch Antenna with Defected Ground Structure for ISM Band, *7th International Conference on Computer and Communication Engineering (ICCCE),* **2018**, pp. 104-108, doi: 10.1109/ICCCE.2018.8539260.
[13] Marqués, R., Martin, F. and Sorolla, M. *Metamaterials with Negative Parameters: Theory, Design, And Microwave Applications*. John Wiley & Sons, **2011**.
[14] Afsar MS, Faruque MR, Abdullah S, et al. An Innovative Compact Split-Ring-Resonator-Based Power Tiller Wheel-Shaped Metamaterial for Quad-Band Wireless Communication. *Materials*. **2023** 28;16(3):1137.
[15] T. Ali, S. A. W. Mohammad, and R. C. Biradar. A novel metamaterial rectangular CSRR with pass band characteristics at 2.95 and 5.23 GHz. *2nd IEEE International Conference on Recent Trends in Electronics, Information & Communication Technology (RTEICT),* **2017**, pp. 256-260, doi: 10.1109/RTEICT.2017.8256597.
[16] Zhang, X., Wu, W., Ma, Y., et al. Design dual-polarization frequency selective rasorber using split ring resonators. *IEEE Access*, **2019**, 7, pp.101139-101146.
[17] Budnarowska M, Rafalski S, Mizeraczyk J. Vector-Field Visualization of the Total Reflection of the EM Wave by an SRR Structure at the Magnetic Resonance. *Energies*. **2021** Dec 24;15(1):111.
[18] Soerbakti Y, Syahputra RF, Gamal MD, et al. Improvement of low-profile microstrip antenna performance by hexagonal-shaped SRR structure with DNG metamaterial characteristic as UWB application. *Alexandria Engineering Journal*. **2022** 1;61(6):4241-52.
[19] Liu S, Wang Z, Dong Y. Compact wideband SRR-inspired antennas for 5G microcell applications. *IEEE Transactions on Antennas and Propagation*. **2021** 6;69(9):5998-6003.
[20] Kaur N, Sivia JS, Kumar M. SRR and rectangular stubs loaded novel fractal antenna realization for multiband wireless applications. *Wireless Personal Communications*. **2021** Sep;120(1):515-33.
[21] Maccartney, G.R., Rappaport, T.S., Sun, S., et al. Indoor office wideband millimeter-wave propagation measurements and channel models at 28 and 73 GHz for ultra-dense 5G wireless networks. *IEEE Access*, **2015**, 3, pp.2388-2424.
[22] Ghosh, S. and Sen, D. An inclusive survey on array antenna design for millimeter-wave communications. *IEEE Access*, **2019**, 7, pp.83137-83161.